Effects of Thickness Variation on the Aeroelastic Performance of Continuous Tow Sheared Composite Wing

Harry J. Leitch*
Department of Mechanical and Aerospace Engineering, University of Strathclyde, Glasgow, G1 1XQ, United Kingdom

Olivia Stodieck†
Dapta Ltd, Bristol, BS1 1LT, United Kingdom

Jie Yuan‡
Department of Aeronautics and Astronautics, University of Southampton, Southampton, SO17 1BJ, United Kingdom

Continuous tow shearing is a promising manufacturing technique which can produce highly tailored steered carbon fibre laminates. This has been shown to improve the buckling resistance and aeroelastic performace of composite structures. One of the differences in the modelling in comparison to conventional laminates is that the thickness depends on how much the fibres are steered. Many optimisation studies use Tsai lamination parameters which cannot these thickness changes in the modelling. This work aims to highlight the importance of including the effect of thickness coupling when modelling the aeroelastic behaviour of continuous tow sheared composites. A semi-analytical plate model was used in this work which has been validated against a finite element model. The effect of thickness variation can be significant but is not uniform therefore neglecting this effect could impact the design optimisation process. The impact on the uncertainty distribution is less significant so lamination parameter could still be used to assess the reliability of layups if corrected using a model which includes thickness coupling.

I. Nomenclature

$\mathbf{A}$	=	mass matrix
$\mathbf{B}$	=	aerodynamic damping matrix
$\mathbf{C}$	=	aerodynamic stiffness matrix
$\mathbf{C}_k$	=	orthotropic matrix of each ply
c	=	chord length
$\mathbf{D}$	=	out-of-plane laminate stiffness matrix, structural damping matrix
η	=	non-dimensional x coordinate
$\mathbf{E}$	=	structural stiffness matrix
E_1	=	longitudinal modulus
E_2	=	transverse modulus
E_k	=	kinetic energy
E_s	=	strain energy
γ	=	structural damping coefficient
G_{12}	=	shear modulus
$\mathbf{I}$	=	identity matrix
λ	=	eigenvalue
L_m, L_n	=	legendre polynomials
ϕ	=	reference angle
$\mathbb{Q}_{ij}$	=	generalised force on plate

*PhD Student, Aerospace Centre of Excellent
†Engineer and Founder
‡Assistant Professor, Computation Engineering Design Group, j.yuan@soton.ac.uk

q_{mn} = generalised coordinates
ρ_0 = density of ply material
s = semi-span
θ = fibre angle
t = time
t_0 = initial thickness of single ply
T_m = angle at reference point
t_m = thickness of manufactured ply
ω = natural frequency
W = work done on plate
w = vertical displacement
ξ = non-dimensional y coordinate
x' = coordinate along reference line
x'_m = reference point
ζ = damping ratio
z_k = thickness coordinate of each ply

II. Introduction

One of the key ways of reducing the fuel consumption of aircraft is to reduce the structural mass as this allows more payload to be carried per unit of fuel. The use of composite materials has allowed recently developed aircraft to significantly reduce their structural weight and provide tailorable mechanical properties for efficient aircraft designs. The design of composite layups in these aircraft tend to be straight fibre quasi-isotropic as these have been extensively tested and perform well under a variety of loading conditions. This type of layup, however, does not make use of the full potential of the composite materials as the layup can be more specifically tailored to the requirements of the structure.

Continuous tow shearing (CTS) allows even further tailoring as the orientation of the fibres can be varied continuously throughout each layer in the laminate[1]. This is achieved through the use of a specialised placement head which changes the direction of the prepreg tape by shearing the tape perpendicular to the direction of the placement head. The main benefits of using CTS composites are improved aeroelastic performance and buckling strength [2] [3]. In a study by Wang et al. [4] it was shown that the mass of a aircraft wing could be reduced by up to 13.2% using CTS instead of a typical quasi-isotropic straight-fibre layup.

Current modelling approaches used in the analysis of CTS structures are largely similar to conventional composites with the main difference being the changes in ply properties throughout the structure. Most studies calculate the laminate properties based on predefined fibre paths for each layer, using classical laminate theory (CLT) [5] or first-order shear deformation theory (FSDT) [6]. This method allows easy application of manufacturing constraints such as maximum shearing angle and fibre bend radius. For thick structures with many layers, the number of variables can become very high, causing design optimisation to become very computationally expensive. As a result, many optimisation studies use Tsai lamination parameters as the stiffness of any laminate can be represented by 12 parameters at each point [7][8][9]. As well as the potential reduction in input parameters, feasible domain in generally convex allowing gradient-based optimisation to be used [10]. Some of the drawbacks include the difficulty in applying manufacturing constraints and the recovery of the fibre path.

The shearing of the fibres during CTS results in an increase in thickness as the angle increases [11]. This effect is often absent in the modelling of CTS laminates which may impact the validity of the design optimisation process. This particularly affects optimisations which use Tsai lamination parameters instead of directly calculating the stiffness from the fibre angles. One of the major implications on the modelling when using this method is that the fibre orientation of each ply is not known during the optimisation. As a result, the thickness coupling due to CTS will not be captured in the modelling as it is dependant on the fibre shearing angle. The effect of this thickness coupling is not necessarily uniform therefore this work will consider a range of layups to assess the consistency of this effect.

Sources of uncertainty is CTS composites are very similar to conventional straight fibre composites. This includes the fibre and matrix properties, volume fraction, ply thicknesses, and fibre angles [12]. Most studies which consider uncertainty quantification in composite materials use Monte Carlo simulations (MCS) to determine the effect on the structural properties [13][14]. It is also common for uncertainty studies to use meta-modelling technique such as Kriging predictors or polynomial chaos expansions to reduce computational efficiency [15][16]. MCS is still often used for validation when using meta-models. Some studies consider the uncertainty in the material properties to be spatially

distributed as properties such as fibre volume fraction may not be constant throughout the structure [17]. In this work it is assumed that the thickness of prepreg carbon fibre tape does not change significantly throughout the plate as the geometry is small but for larger structure this effect may be more important.

This work aims to highlight the the issues present when using lamination parameters in the modelling and/or optimisation of CTS composites structures. The main contribution of this work is is a comprehensive comparison of the aeroelastic response when the shear induced thickness coupling is includes against a model without thickness coupling. This will include the deterministic flutter/divergence speed of 25 layups and the response under thickness uncertainty for 3 layups. A semi-analytical flat plate model will be used to make this comparison. This model was first validated against a finite element model (FEM) then the deterministic results will be presented. The flutter speed distribution of the 3 uncertain cases will then be presented. Additionally, the impact of each thickness will be assessed using Sobol indices, with and without thickness coupling.

III. Methodology

The model used in this test case is a rectangular flat plate fixed at one end shown in Fig. 1 which allows the semi-analytical Rayleigh Ritz (RR) method [18][19] to be implemented. A FEM was also developed for the same test case to validate the implementation of the RR model.

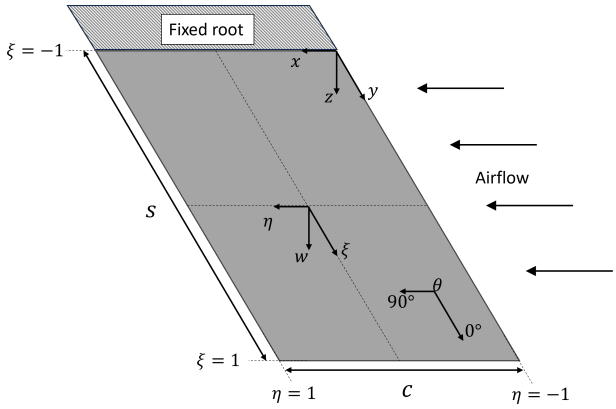

Fig. 1 Flat plate model

For the RR model, non-dimensional coordinates were used in place of x and y as seen in Eq. (1) to simplify the derivation and implementation of the method.

$$\xi(y) = \frac{2y}{s} - 1 \quad ; \quad \eta(x) = \frac{2x}{c} - 1 \tag{1}$$

A. CTS composite Modelling

The stiffness matrix at each point of the laminate was determined using CLT [20] [21] where the fibre angle and thickness in each ply was dependent on the position in the x-y plane. The fibre orientation was defined as a variation in angle with respect to a reference line x', as see in Fig. 2. As previously mentioned, the fibre angle will only be varied in the span-wise direction so x' will be aligned with the y axis. The fibre angle distribution in each ply is calculated using a Lagrange basis polynomial function shown in Eq. (2) where T_m is the angle at each reference point x'_m.

$$\theta(x, y) = \phi + \theta(x') = \phi + \sum_{m=0}^{M-1} T_m \prod_{m \neq i} \left(\frac{x' - x'_i}{x'_m - x'_i} \right) \tag{2}$$

This paper will only use 2 reference angle for each CTS ply which results in a linear distribution in the fibre angle along the span of the plate. The test case also only uses CTS for the outer 2 plies on each side of the plate and is symmetrical, therefore only 4 CTS reference angles are required for each layup. These reference angles are expressed in the following form.

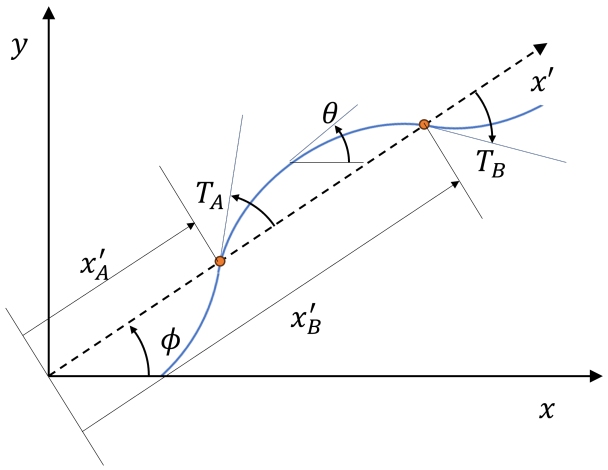

Fig. 2 Fibre angle variation

$$< T_{11}, T_{12} >, < T_{21}, T_{22} > \tag{3}$$

Where T_{11} and T_{12} are the fibre orientations at the root and tip of ply 1 and 8, and T_{21} and T_{22} are the fibre orientations at the root and tip of ply 2 and 7.

The shearing of the fibre tape induces changes in fibre thickness as shown in Fig. 3 and the thickness of each ply at each point is calculated using Eq. (4).

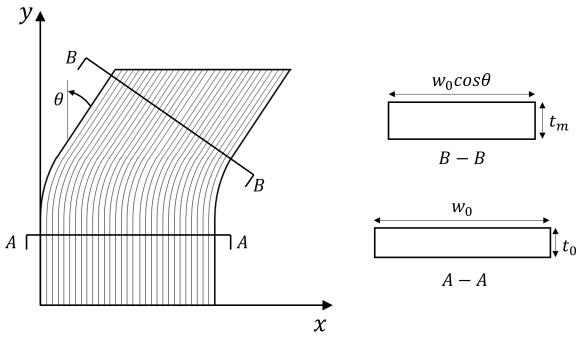

Fig. 3 Thickness coupling due to shearing

$$t_m = \frac{t_0}{cos(\theta)} \tag{4}$$

This change in thickness is taken into account when calculating the terms in the laminate stiffness matrix at each point on the plate. As seen in Eq. (5) where the D matrix terms have a cubic relationship to the ply thickness and position from mid plane. The total thickness of the laminate is calculated including this variation when generating the mass matrix in the RR method.

$$\mathbf{D} = \sum_{k=1}^{n} \mathbf{D}_k = \frac{1}{3} \sum_{k=1}^{n} \mathbf{C}_k \left((z_k)^3 - (z_{k-1})^3 \right) \tag{5}$$

Where $\mathbf{C}_k$ is the orthotropic stiffness matrix of each ply and z_k is the thickness coordinate of each ply relative to the mid-plane.

B. Rayleigh Ritz Aeroelastic Model

The RR method is commonly used for modelling simple problems in a semi analytical way by defining the deformation in terms of a set of shape functions. This allows the formulation of eigenvalue problems in terms of these shape function which can significantly reduce the number of degrees of freedom in the problem. The shape functions used are based on Legendre polynomials which allow out of plane deformations which vary across the x-y plane, as see in Eq. (6). The shape functions are also used to enforce the boundary conditions through the addition of the $(1+\xi)^2$ term.

$$w(\xi,\eta) = \sum_{m=0}^{m_{max}} \sum_{n=0}^{n_{max}} q_{mn}(1+\xi)^2 L_m(\xi) L_n(\eta) \tag{6}$$

Lagrange's energy equations were used to derive the coupled aerodynamic model with the kinetic energy defined in Eq. (8) and the strain energy defined in Eq. (9). The formulation of the strain energy equation assumes the in-plane deformations and chord-wise bending are negligible compared to the span-wise bending and torsion deformations. It is important to note that the thickness t and the stiffness terms D_{11}, D_{16}, D_{66} vary with x and y therefore E_k and E_s were integrated numerically. The aerodynamic loads represented by $\mathbb{Q}_{ij}$ are based on quasi-steady aerodynamics [22].

$$\frac{d}{dt}\left(\frac{\partial E_k}{\partial \dot{q}_{ij}}\right) - \frac{\partial E_k}{\partial q_{ij}} + \frac{\partial \gamma}{\partial \dot{q}_{ij}} + \frac{\partial E_s}{\partial q_{ij}} = \mathbb{Q}_{ij} = \frac{\partial(\delta W)}{\partial(\delta q_{ij})} \tag{7}$$

$$E_k = \frac{1}{2}\iint \rho_0 t(x,y)\dot{w}^2 \, dx\, dy \tag{8}$$

$$E_s = \frac{1}{2}\iint D_{11}(x,y)\left(\frac{\partial^2 w}{\partial y^2}\right)^2 + 4D_{16}(x,y)\left(\frac{\partial^2 w}{\partial y^2}\right)\left(\frac{\partial^2 w}{\partial x \partial y}\right) + 4D_{66}(x,y)\left(\frac{\partial^2 w}{\partial x \partial y}\right)^2 dx\, dy \tag{9}$$

$$\mathbf{A}\ddot{q} + (\rho V \mathbf{B} + \mathbf{D})\dot{q} + (\rho V \mathbf{C} + \mathbf{E})q = 0 \tag{10}$$

$$\begin{Bmatrix} \dot{q} \\ \ddot{q} \end{Bmatrix} = \begin{bmatrix} 0 & \mathbf{I} \\ -\mathbf{A}^{-1}(\rho V \mathbf{C} + \mathbf{E}) & -\mathbf{A}^{-1}(\rho V \mathbf{B} + \mathbf{D}) \end{bmatrix} \begin{Bmatrix} q \\ \dot{q} \end{Bmatrix} \tag{11}$$

The first order matrix form of the Lagrange's equations seen in Eq. (11) was solved as an eigenvalue problem for each case (different layup and airspeed). The resulting eigenvalues are in the form shown in Eq. (12) which were use to determine the natural frequencies and damping ratios. For each layup the flutter or divergence speed was determined by solving for the lowest input velocity which resulted in a damping ratio of 0.

$$\lambda_{ij} = -\zeta_{ij}\omega_{ij} \pm i\omega_{ij}\sqrt{1-\zeta_{ij}^2} \tag{12}$$

C. Finite Element Model

An FEM was generated using NASTRAN with a mesh consisting of 240 4-node quadrilateral shell (CQUAD4) elements. The variation in fibre orientation and thickness was calculate at the centroid of each element using the same definition as in Sec. III.A. with the properties in each element defined using PCOMP cards. To ensure the comparison between the FEM and RR model was fair, a set of chord-wise stiffeners were added as mass-less rigid beam elements (RBE1), as seen in Fig. 4.

Modal analysis (SOL 103) was performed to find the natural frequencies and mode shapes of the plate with no aerodynamic forces to allow the structural model to be compared to the RR model. The first 5 natural frequencies for a set of 25 different layups were obtained and The modal assurance criterion (MAC) [23] was used to compare the correlation of the mode shapes obtained in each model. A NASTRAN solver (SOL 145) was also used to validate aeroelastic response of the RR model, which used doublet lattice aerodynamics [24] and the PK method [18].

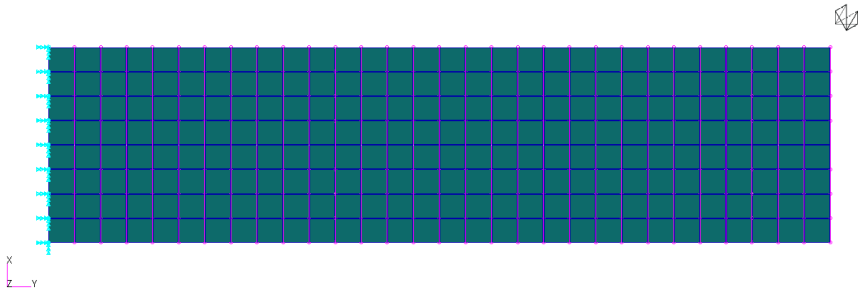

Fig. 4 FEM mesh with rigid beam elements shown in pink

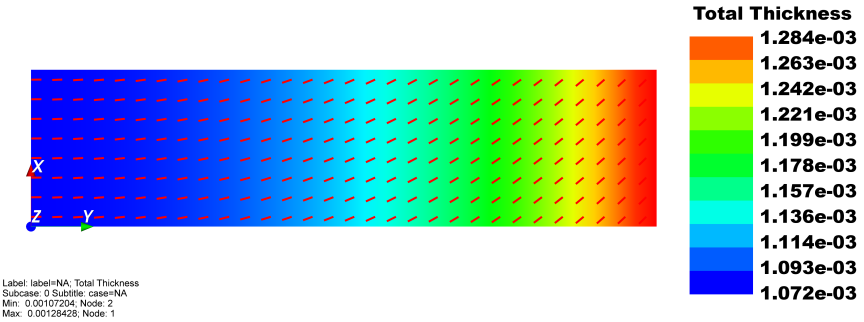

Fig. 5 Thickness and fibre angle variation

D. Uncertainty Quantification

A uniform distribution of ±5% was applied to the nominal thickness (t_0) of each of the 8 plies [13][25]. Monte Carlo sampling was used to determine the distribution of flutter/divergence speed due to the thickness uncertainty. Probability distribution functions (PDFs) were generated from the output samples and the mean and coefficient of variance (COV) were calculated. The output distributions with and without the effect of thickness coupling were compared.

To determine the influence of each thickness uncertainty on the flutter/divergence speed, Sobol analysis will be performed [26][27]. The formulation of the Sobol indices are show in Eq. (13)-(16) which requires 2 sets of sample points $X^{(1)}$ and $X^{(2)}$.

$$U_i = \frac{1}{N}\sum_{k=1}^{N} Y^k(X_k^{(1)}) \times Y^k(X_k^{(2)}) \tag{13}$$

$$S_i = \frac{U_i - \mu^2}{\sigma^2} \tag{14}$$

$$S_{Ti} = S_i + \sum_{j=1, j\neq i}^{n} S_{ij} \tag{15}$$

$$S_{ij} = \frac{Var[\mathbb{E}[Y^k|X_i, X_j]]}{\sigma^2} \tag{16}$$

Where S_i is the first order order Sobol index which represents the influence of each variable without interaction with the others and S_{Ti} is the total order Sobol index which represents the influence of each variable including interaction with the other variables.

Due to the high number of samples required to achieve convergence when performing Sobol analysis, a Kriging model will be developed for each layup. The samples generated during the uncertainty quantification were used to train the Kriging model [28][29]. The formulation of the Kriging model is shown in Eq. (17)-(18).

$$P(x) = \mu(x) + \mathbf{w}^T(x)K^{-1}(Y - \mu(X)) \tag{17}$$

Where $\mu(x)$ is the expected value and K is a covariance matrix which represents the correlation between the training data points. The weight factor $\mathbf{w}(x)$ depends on the correlation between the input to be estimated and the training data

$$\mathbf{w}(x) = K^{-1} Corr(x, X) \tag{18}$$

The accuracy of the Kriging models were verified by comparing it against an independent set of 200 samples. OpenTURNS was used to generate input and output distributions, to generate Kriging models, perform sensitivity analysis and plot results [30].

IV. Results and Discussion

The test case will use an 8 ply symmetric layup with 4 inner plies using straight fibre with a [45, -45]s layup and the fibre angles of outer 2 plies on each side will vary only in the span-wise direction . The dimensions and material properties used in the test case are shown in Tab. 1 which are based on the typical properties of a unidirectional carbon fibre composite.

Table 1 Material properties

c	$76.2mm$
s	$304.8mm$
t_0	$0.134mm$
ρ_0	$1520kg/m^3$
E_1	$98000MPa$
E_2	$7900MPa$
G_{12}	$5600MPa$
υ_{12}	0.28

A. Validation of Rayleigh Ritz Model

The first 3 mode shapes for a <0,45>, <0,-45> layup were compared using both models, which as seen in Fig. 7 matched well. The first mode is a pure bending mode, the 2nd mode is a torsion mode and the third mode includes bending and torsion.

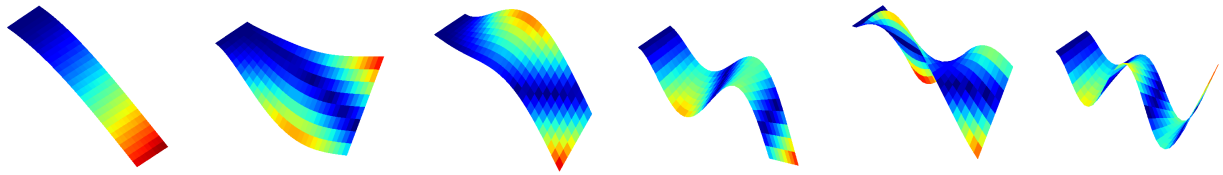

Fig. 6 Mode shapes using RR model for <0,45>, <0,-45> layup

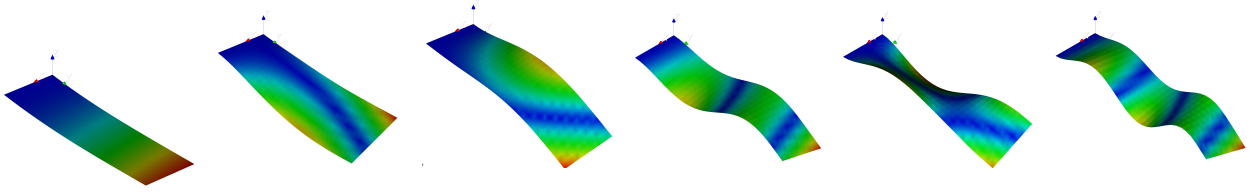

Fig. 7 Mode shapes using FEM for <0,45>, <0,-45> layup

To ensure the validity of the structural model implemented in the RR method, the natural frequencies and mode shapes were validated against the FEM. A set of 25 design points were used to generate results for each method and the first 5 natural frequencies were compared. As seen in Tab. 2, the average error in the first 5 natural frequencies are very low with only 2 modes modes exceeding 1% in the average error. The maximum errors obtained are also low with the highest being only 4.42%.

Table 2 % error in natural frequencies between RR and FEM

Mode no.	1	2	3	4	5
Average	0.27%	0.75%	1.17%	1.32%	0.82%
Max	0.78%	1.52%	2.82%	4.42%	2.00%
Min	0.00%	0.06%	0.20%	0.05%	0.03%
SD	0.21%	0.38%	0.73%	1.40%	0.88%

To compare the mode shapes 3 different layups were used to generate MAC matrices, as seen in Fig. 8a, 8b and 8c. The MAC values were only calculated using the first 6 modes as these account for over 90% of the modal effective mass. The correlation of mode shape between the RR and FEM models is strong, with high mac values for corresponding modes and very low values for the others.

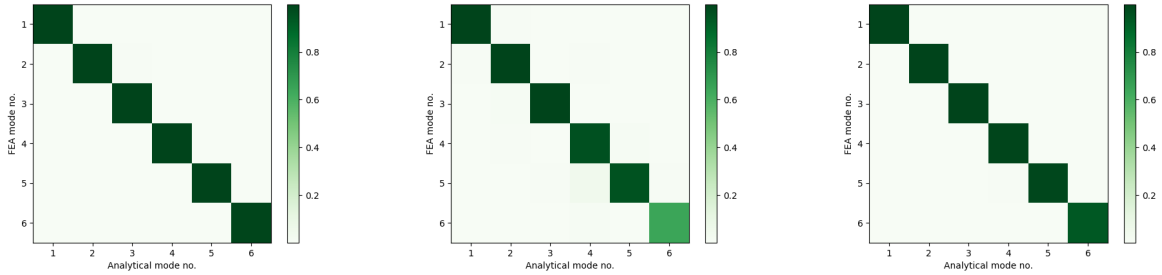

(a) <0,45>, <0,-45> layup **(b) <30,-10>, <-45,-20> layup** **(c) <-30,0>, <20,45> layup**

Fig. 8 MAC values for three different CTS layups

The same 3 layups were used to validate the RR aeroelastic model against the NASTRAN FEM model. As seen in Fig. 9, the aeroelastic responses were very similar. The main difference was the damping ratio when the frequency was zero as NASTRAN changes to a real eigenvalue solution instead of a complex one. Despite this difference, the divergence speed of these layups matched well.

B. Thickness coupling results

As seen in Fig. 10, the thickness coupling due to shearing can result in in a significant increase in aeroelastic performance as there is a 10m/s (17.5%) increase in divergence speed. There is also a clear increase in the natural frequency due to the thickness coupling. To assess the effect of thickness coupling on the aeroelastic performance for different layups, the flutter/divergence speed was evaluated for the same 25 layups used in Sec. IV.A. There was an average increase of 6.51% in flutter/divergence speed. The increase in flutter/divergence speed also appears to be highly dependant on the layup as the was significant variation in the results ranging from 0.91% to 61%. The standard deviation of the sample was 11.66% further highlighting the variable impact of including thickness coupling.

C. Thickness uncertainty results

To ensure the number of samples in the uncertainty quantification was sufficient, the samples, mean value and standard deviation were plotted to check for convergence. As seen in Fig. 11a, the output distribution was converged by 1000 samples. The Kriging models were validated against a set of 200 independent samples which showed very good correlation, seen in Fig. 11b.

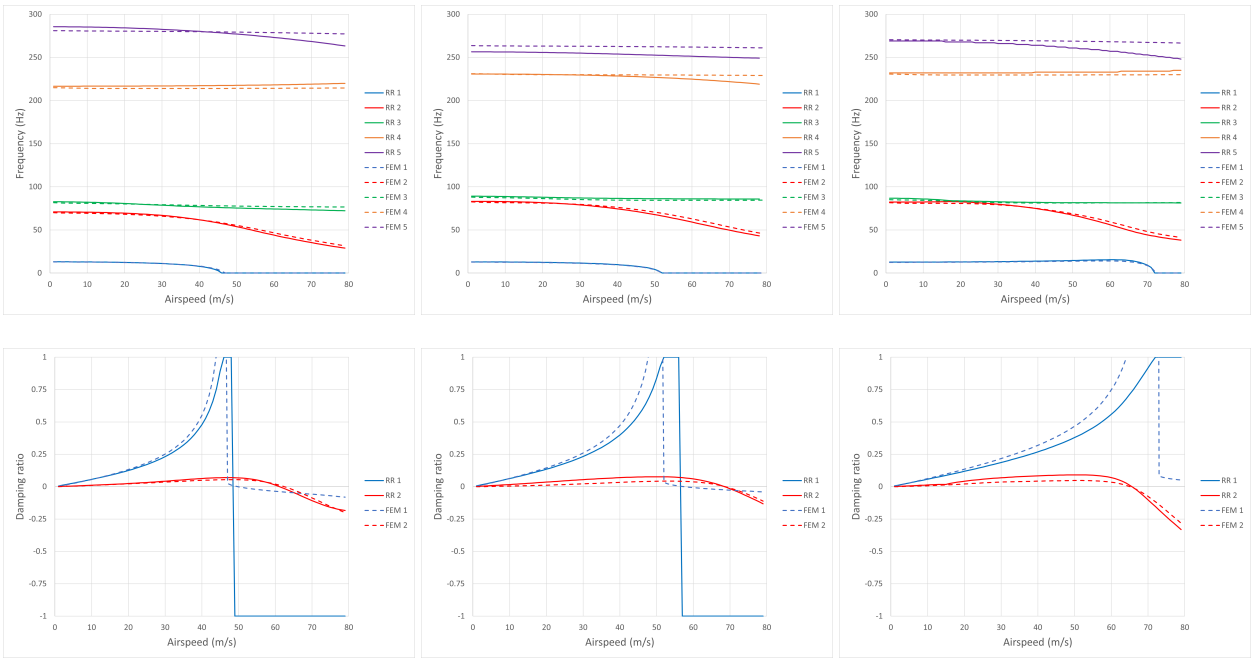

(a) <0,45>, <0,-45> layup **(b) <30,-10>, <-45,-20> layup** **(c) <-30,0>, <20,45> layup**

Fig. 9 Aeroelastic response for three different CTS layups

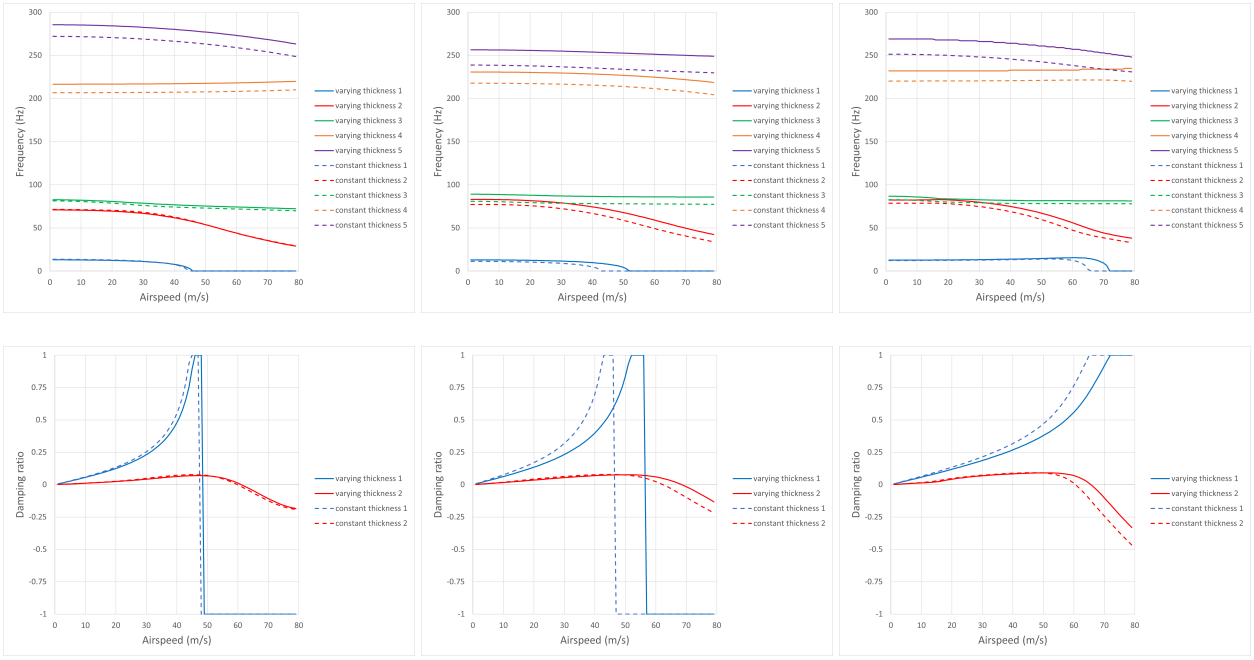

(a) <0,45>, <0,-45> layup **(b) <30,-10>, <-45,-20> layup** **(c) <-30,0>, <20,45> layup**

Fig. 10 Natural frequencies and damping ratios for three different CTS layups, with (solid line) and without thickness coupling (dashed line)

As seen in Fig. 12, the PDFs with and without thickness coupling are similar with their distributions offset from each other, with the largest difference of the <30,-10>, <-45,-20> layup. This matches well with the deterministic results seen in Fig. 10. For cases (b) and (c), the difference in the mean is similar or larger than the uncertainty range so the

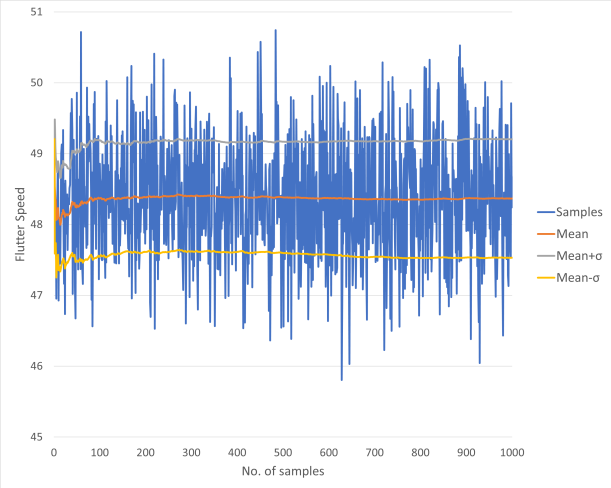

(a) Uncertainty quantification convergence

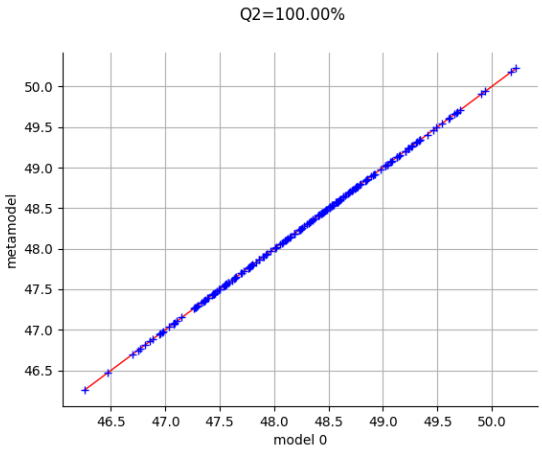

(b) Kriging model validation

Fig. 11 for <0,45>, <0,-45> layup

effect thickness coupling cannot be neglected. The difference in the COV is also very small, with the largest difference for the <30,-10>, <-45,-20> layup, which decreased from 0.0221 to 0.0202 when thickness coupling was removed. This suggests that the inclusion of thickness coupling has little effect on assessing the reliability of a particular layup as only the mean values were significantly impacted.

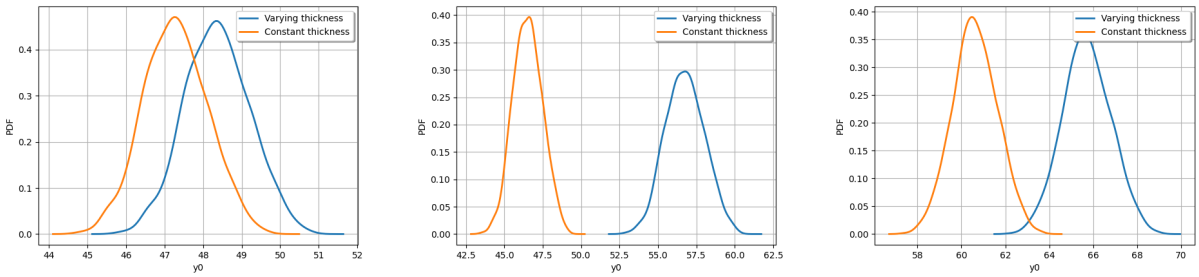

(a) <0,45>, <0,-45> layup **(b) <30,-10>, <-45,-20> layup** **(c) <-30,0>, <20,45> layup**

Fig. 12 Flutter speed distributions for three different CTS layups

As seen in Fig. 13, the 2nd ply from the top and bottom have the largest effect on the flutter speed for the <0,45>, <0,-45> layup, with the outermost ply having very little effect and the core plies having a moderate effect. The influence of each ply thickness is almost entirely 1st order suggesting that there is very little interaction between the ply thicknesses. The Sobol indices are also very similar with and without thickness coupling further showing that it has little effect on assessing the impact of uncertainty.

V. Conclusion

Neglecting the shear induced thickness variations in the aeroelastic analysis of CTS structure can result in significant under prediction of the flutter and divergence speed. This effect is not uniform across the design space so will have a significant impact on modelling using lamination parameters. As a result, the use of lamination as input parameters in the design of CTS laminates is not be suitable as it may result in layups which benefit from the thickness coupling being ignored in the optimisation. The result of this will be a sub-optimal layup or very conservative design. The impact on stochastic modelling is not as significant as the coefficient of variance is not significantly impacted. As a result, the PDF around a known layup could be estimated using lamination parameters which can then be corrected

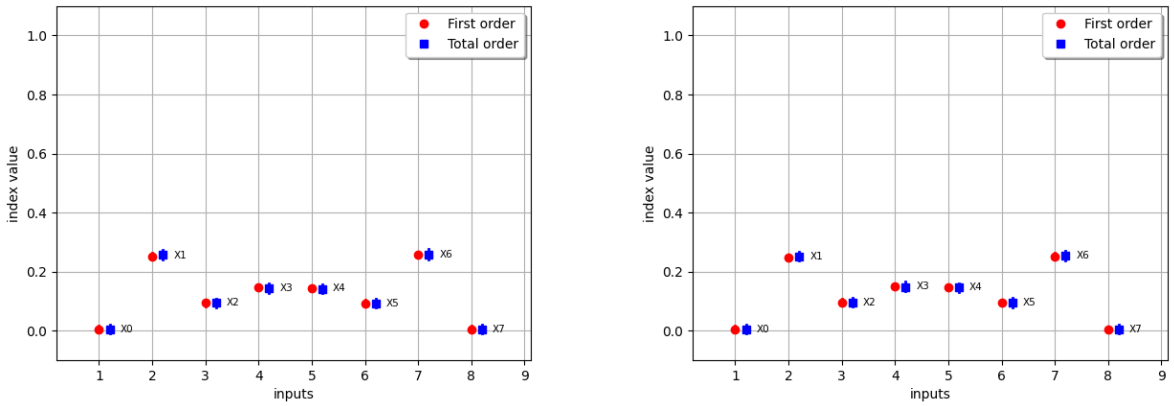

(a) With thickness coupling **(b) Without thickness coupling**

Fig. 13 Sobol indices for <0,45>, <0,-45> layup (inputs are ply thicknesses from top to bottom of plate)

using the deterministic result using fibre angles as the inputs. This will reduce the number of inputs in the uncertainty quantification, reducing the computational expense. More work will be required to ensure the impact of excluding thickness coupling on uncertainty quantification similar across the rest of the design space for CTS laminates.

Acknowledgments

H. Leitch acknowledges the support of the Strathclyde Research Studentship Scheme, Dapta Ltd. and National Manufacturing Institute Scotland. J.Yuan acknowledges the funding support of the Royal Academy of Engineering/Leverhulme Trust Research Fellowship (LTRF2223-19-150).

References

[1] Kim, B. C., Potter, K., and Weaver, P. M., "Continuous tow shearing for manufacturing variable angle tow composites," *Composites Part A: Applied Science and Manufacturing*, Vol. 43, No. 8, 2012, pp. 1347–1356. https://doi.org/10.1016/j.compositesa.2012.02.024.

[2] Stodieck, O., "Aeroelastic Tailoring of Tow-Steered Composite Wings," Ph.D. thesis, University of Bristol, 2016. https://doi.org/10.13140/RG.2.2.29020.82562.

[3] Lincoln, R., Weaver, P., Pirrera, A., and Groh, R., "Optimisation of continuous tow-sheared cylinders under uncertainty," 2021.

[4] Wang, Z., Wan, Z., Groh, R. M., and Wang, X., "Aeroelastic and local buckling optimisation of a variable-angle-tow composite wing-box structure," *Composite Structures*, Vol. 258, 2021, p. 113201. https://doi.org/https://doi.org/10.1016/j.compstruct.2020.113201.

[5] Racionero Sánchez-Majano, A., and Pagani, A., "Buckling and Fundamental Frequency Optimization of Tow-Steered Composites Using Layerwise Structural Models," *AIAA Journal*, Vol. 61, No. 9, 2023, pp. 4149–4163. https://doi.org/10.2514/1.J062976.

[6] Montemurro, M., "An extension of the polar method to the First-order Shear Deformation Theory of laminates," *Composite Structures*, Vol. 127, 2015, pp. 328–339. https://doi.org/https://doi.org/10.1016/j.compstruct.2015.03.025.

[7] Tsai, S., Pagano, N., and OHIO., A. F. M. L. W.-P. A., *Invariant Properties of Composite Materials*, Defense Technical Information Center, 1968.

[8] Macquart, T., Maes, V., Bordogna, M. T., Pirrera, A., and Weaver, P., "Optimisation of composite structures – Enforcing the feasibility of lamination parameter constraints with computationally-efficient maps," *Composite Structures*, Vol. 192, 2018, pp. 605–615. https://doi.org/https://doi.org/10.1016/j.compstruct.2018.03.049.

[9] Albazzan, M. A., Harik, R., Tatting, B. F., and Gürdal, Z., "Efficient design optimization of nonconventional laminated composites using lamination parameters: A state of the art," *Composite Structures*, Vol. 209, 2019, pp. 362–374. https://doi.org/https://doi.org/10.1016/j.compstruct.2018.10.095.

[10] Bloomfield, M. W., Diaconu, C. G., and Weaver, P. M., "On Feasible Regions of Lamination Parameters for Lay-Up Optimization of Laminated Composites," *Proceedings: Mathematical, Physical and Engineering Sciences*, Vol. 465, No. 2104, 2009, pp. 1123–1143.

[11] Kim, B. C., Weaver, P. M., and Potter, K., "Manufacturing characteristics of the continuous tow shearing method for manufacturing of variable angle tow composites," *Composites Part A: Applied Science and Manufacturing*, Vol. 61, 2014, pp. 141–151. https://doi.org/https://doi.org/10.1016/j.compositesa.2014.02.019.

[12] Mesogitis, T., Skordos, A., and Long, A., "Uncertainty in the manufacturing of fibrous thermosetting composites: A review," *Composites Part A: Applied Science and Manufacturing*, Vol. 57, 2014, pp. 67–75. https://doi.org/https://doi.org/10.1016/j.compositesa.2013.11.004.

[13] Kumar, D., Koutsawa, Y., Rauchs, G., Marchi, M., Kavka, C., and Belouettar, S., "Efficient uncertainty quantification and management in the early stage design of composite applications," *Composite Structures*, Vol. 251, 2020, p. 112538. https://doi.org/https://doi.org/10.1016/j.compstruct.2020.112538.

[14] Dodwell, T., Kynaston, S., Butler, R., Haftka, R., Kim, N. H., and Scheichl, R., "Multilevel Monte Carlo simulations of composite structures with uncertain manufacturing defects," *Probabilistic Engineering Mechanics*, Vol. 63, 2021, p. 103116. https://doi.org/https://doi.org/10.1016/j.probengmech.2020.103116.

[15] Zhou, C., Li, C., Zhang, H., Zhao, H., and Zhou, C., "Reliability and sensitivity analysis of composite structures by an adaptive Kriging based approach," *Composite Structures*, Vol. 278, 2021, p. 114682. https://doi.org/https://doi.org/10.1016/j.compstruct.2021.114682.

[16] Scarth, C., Cooper, J. E., Weaver, P. M., and Silva, G. H., "Uncertainty quantification of aeroelastic stability of composite plate wings using lamination parameters," *Composite Structures*, Vol. 116, 2014, pp. 84–93. https://doi.org/https://doi.org/10.1016/j.compstruct.2014.05.007.

[17] Guimarães, T. A. M., Silva, H. L., Rade, D. A., and Cesnik, C. E. S., "Aeroelastic Stability of Conventional and Tow-Steered Composite Plates Under Stochastic Fiber Volume," *AIAA Journal*, Vol. 58, No. 6, 2020, pp. 2748–2759. https://doi.org/10.2514/1.J059106.

[18] Wright, J., and Cooper, J., *Introduction to aircraft aeroelasticity and loads.*, John Wiley & Sons, 2008.

[19] Stodieck, O., Cooper, J. E., Weaver, P. M., and Kealy, P., "Improved aeroelastic tailoring using tow-steered composites," *Composite Structures*, Vol. 106, 2013, pp. 703–715. https://doi.org/https://doi.org/10.1016/j.compstruct.2013.07.023.

[20] Öchsner, A., *Foundations of Classical Laminate Theory*, Springer International Publishing, Cham, 2021, Chap. Macromechanics of a Laminate, pp. 41–50. https://doi.org/10.1007/978-3-030-82631-4_3, URL https://doi.org/10.1007/978-3-030-82631-4_3.

[21] DONG, S. B., PISTER, K. S., and TAYLOR, R. L., "On the Theory of Laminated Anisotropic Shells and Plates," *Journal of the Aerospace Sciences*, Vol. 29, No. 8, 1962, pp. 969–975. https://doi.org/10.2514/8.9668.

[22] YATES, E. C., "Modified-strip-analysis method for predicting wing flutter at subsonic to hypersonic speeds." *Journal of Aircraft*, Vol. 3, No. 1, 1966, pp. 25–29. https://doi.org/10.2514/3.43702.

[23] Pastor, M., Binda, M., and Harčarik, T., "Modal Assurance Criterion," *Procedia Engineering*, Vol. 48, 2012, pp. 543–548. https://doi.org/10.1016/j.proeng.2012.09.551.

[24] ALBANO, E., and RODDEN, W. P., "A doublet-lattice method for calculating lift distributions on oscillating surfaces in subsonic flows." *AIAA Journal*, Vol. 7, No. 2, 1969, pp. 279–285. https://doi.org/10.2514/3.5086.

[25] Tomblin, J., McKenna, J., and Y. Ng, K. S. R., "Advanced General Aviation Transport Experiments:B – Basis Design Allowables for Epoxy – Based Prepreg Newport Graphite Unitape G150 NASS / NCT321," Tech. rep., National Institute for Aviation Research, 2001.

[26] Sobol', I., "Global sensitivity indices for nonlinear mathematical models and their Monte Carlo estimates," *Mathematics and Computers in Simulation*, Vol. 55, No. 1, 2001, pp. 271–280. https://doi.org/https://doi.org/10.1016/S0378-4754(00)00270-6.

[27] Saltelli, A., "Making best use of model evaluations to compute sensitivity indices," *Computer Physics Communications*, Vol. 145, No. 2, 2002, pp. 280–297. https://doi.org/https://doi.org/10.1016/S0010-4655(02)00280-1.

[28] Sudret, B., "Global sensitivity analysis using polynomial chaos expansions," *Reliability Engineering & System Safety*, Vol. 93, No. 7, 2008, pp. 964–979. https://doi.org/https://doi.org/10.1016/j.ress.2007.04.002.

[29] Cressie, N., "The origins of kriging," *Mathematical Geology*, Vol. 22, 1990, pp. 239–252.

[30] Baudin, M., Dutfoy, A., Iooss, B., and Popelin, A.-L., *OpenTURNS: An Industrial Software for Uncertainty Quantification in Simulation*, Springer International Publishing, Cham, 2016, pp. 1–38. https://doi.org/10.1007/978-3-319-11259-6_64-1, URL https://doi.org/10.1007/978-3-319-11259-6_64-1.